Catalysis Today 159 (2011) 12–24

Contents lists available at ScienceDirect

Catalysis Today

journal homepage: www.elsevier.com/locate/cattod

Development of dry reforming catalysts at elevated pressure: D-optimal *vs*. full factorial design

Steven Corthals, Toon Witvrouwen, Pierre Jacobs*, Bert Sels*

K.U. Leuven, Centre for Surface Chemistry and Catalysis, Kasteelpark Arenberg 23, 3001 Heverlee, Belgium

ARTICLE INFO

Article history:
Available online 21 July 2010

Keywords:
CO_2 reforming
Dry reforming
Design of experiment
High-throughput experimentation
D-optimal
Full factorial

ABSTRACT

In this paper high-throughput and combinatorial strategies are used to investigate the development of dry reforming catalysts at elevated pressure (7 bar). Via a design of experiment (DoE) two straightforward search strategies, D-optimal and full factorial, were evaluated in their ability to identify highly active and selective catalysts.

An extensive high-throughput screening has pointed out that Ni and $MgAl_2O_4$ were the active element and support, respectively, with the highest potential for the dry reforming reaction at elevated pressure. A promoter screening of alkaline, alkaline-earth, transition and lanthanide metal oxides on $NiMgAl_2O_4$ catalysts showed that promoter effects, reported at atmospheric pressure, not always hold at elevated pressure. La_2O_3, Y_2O_3 and ZrO_2 were selected as promoters for further use in DoE. A cubic space, constructed with elements with high potential, was explored by the two search strategies. ANOVA analyses of the experimental data resulted in linear equations for the conversions of CH_4 (X_{CH_4}), CO_2 (X_{CO_2}) and the H_2/CO ratio.

Both strategies allowed predicting comparable catalytic results in the major part of the cubic space and deducing the same effects on activity and selectivity for the three selected promoter elements. La_2O_3 affected activity and selectivity in a positive way, while the other two promoters, ZrO_2 and Y_2O_3, resulted in a decreased catalyst performance. Based on the linear equations an objective function *R* was created to determine the most active and selective catalysts. Maximum *R* values were obtained for the same catalyst composition in case of the two different search strategies, hereby demonstrating the advantage of the D-optimal strategy over the full factorial strategy, since in the former case comparable results are obtained with only half of the number of experiments.

1. Introduction

In the last decade dry reforming of CH_4 (1) for the production of synthesis gas regained interest due to the increasing concern of global warming and oil depletion [1–6]. Compared to steam reforming (2), which typically yields a syngas H_2/CO molar ratio of 3, dry reforming (DR) results in synthesis gas with a H_2/CO ratio of 1, suitable for use in the direct production of dimethylether [2,7], hydroformylation, *viz*. propene to *n*-butanal and isobutanal [8], carbonylation, *viz*. methanol to acetic acid [9], and Fischer–Tropsch synthesis [1]. Another area of application for DR is energy-related processes. Its application in solid oxide fuel cells (SOFC) [10] and, due to its high endothermicity, in the thermo-chemical heat pipe reaction process (TCHP) [2] has been investigated.

$$CH_{4(g)} + CO_{2(g)} \leftrightarrow 2CO_{(g)} + 2H_{2(g)} \quad \Delta H_{298} = 247\ \text{kJ/mol} \quad (1)$$

$$CH_{4(g)} + H_2O_{(g)} \leftrightarrow CO_{(g)} + 3H_{2(g)} \quad \Delta H_{298} = 206\ \text{kJ/mol} \quad (2)$$

$$CO_{2(g)} + H_{2(g)} \leftrightarrow H_2O_{(g)} + CO_{(g)} \quad \Delta H_{298} = 41\ \text{kJ/mol} \quad (3)$$

$$2CO_{(g)} \leftrightarrow CO_{2(g)} + C_{(s)} \quad \Delta H_{298} = -172\ \text{kJ/mol} \quad (4)$$

$$CH_{4(g)} \leftrightarrow 2H_{2(g)} + C_{(s)} \quad \Delta H_{298} = 75\ \text{kJ/mol} \quad (5)$$

DR's high endothermicity is the subject of current criticism on dry reforming, pointing to the lack of competitiveness of DR with conventional steam reforming (2). Only for the production of H_2 this statement is valid, since 69 and 124 kJ is needed to produce 1 mole H_2 by steam and DR, respectively. However, for the production of CO this statement does not hold anymore. Taking into account the true reaction temperature (700 °C) and the liquid state of the feed in case of steam reforming, only 130 kJ is required to produce 1 mole of CO in case of DR compared to 221 kJ for steam reforming. These conclusions hold when the heat needed to heat up the feed as well as the heat recovered by cooling down the product mixture are

* Corresponding authors. Fax: +32 16 32 1998.
E-mail addresses: pierre.jacobs@biw.kuleuven.be (P. Jacobs), bert.sels@biw.kuleuven.be (B. Sels).

0920-5861/$ – see front matter © 2010 Elsevier B.V. All rights reserved.
doi:10.1016/j.cattod.2010.06.021

taken into account. Detailed calculations can be found in the first section of the supporting information.

The DR reaction (1) offers the opportunity to convert two abundant greenhouse gases into valuable products. In addition, it allows using alternative carbon sources like natural (CH_4) and biogas (a mixture of CH_4 and CO_2), thus replacing crude oil as carbon feedstock. The reverse water-gas shift (RWGS) reaction (3), the Boudouard reaction (4) and the CH_4 decomposition reaction (5) are assumed to be important side reactions in DR chemistry, as they determine the overall selectivity of the DR process. More importantly, the latter two reactions have a great influence on catalyst lifetime, as they cause coking of the catalyst. Coke may plug the reactor, deactivate the catalyst or cause catalyst pellet destruction. Next to coking also sintering limits catalyst lifetime [1]. High temperatures, required for high equilibrium conversion in DR, and formation of H_2O by the RWGS reaction (3) make catalysts prone to sintering with formation of large metal particles. As the critical metal size needed for catalyzing DR is smaller than for carbon formation [11], sintering will result in increased amounts of carbon residues.

DR has mainly been investigated at atmospheric pressure using various supported catalysts, some of them showing promising catalytic performance [12–15]. High conversions of CO_2 and CH_4, approaching thermodynamic equilibrium, can be obtained over many of them. Noble metal catalysts are reported to be less sensitive to coking compared to Ni catalysts. High cost and low availability of these noble metals, however favor using Ni based catalysts. Industrially, DR will be performed at elevated pressures (>1 bar) to minimize operational costs since consecutive transformations of formed syngas via WGS, Fischer–Tropsch or alcohol synthesis will be performed at elevated pressure. Moreover, it is clear that knowledge on catalyst performance at atmospheric pressure will not always allow extrapolation to elevated pressure. Nagaoka et al. showed for Ru catalysts supported on MgO, Al_2O_3, TiO_2 or SiO_2 that at atmospheric pressure catalyst activity was linked to support basicity ($MgO > Al_2O_3 > TiO_2 > SiO_2$), while at elevated pressures the activity order of the different Ru catalysts ($SiO_2 > Al_2O_3 > MgO > TiO_2$) was related to the specific support BET surface area [16].

Despite the necessity to study DR at elevated pressure, only a limited number of publications is available compared to the abundant number of publications at atmospheric pressure. Supported non-noble (Ni, Co), noble metal (Pt, Ir, Rh, Pd, Ru) or mixed metal catalysts have been reported as catalysts at elevated pressure [16–21], with Al_2O_3, MgO, TiO_2, SiO_2, $SrCO_3$, CeO_2, ZrO_2 serving as support. Moreover, supported or bulk metal carbides of group V (V, Nb, Ta) and VI (W, Mo) of the transition metals seem potential high pressure alternatives for group VIII metals [22–25]. Carbides reported to be stable only at elevated pressure (>8 bar) and high temperature (>800 °C), are capable of mimicking the behavior of group VIII metals [26]. The effect of promoters, essential for a DR catalyst in high-pressure processes, has only occasionally been investigated. To improve the performance of a Pt/ZrO_2 catalyst, only the use of bimetal catalysts and a CeO_2 promoter was reported [17,18].

Given the limited number of DR reports at elevated pressure, we initiated an extensive catalyst development study and an extensive screening of active elements, promoters and support materials. Subsequently, the most active and selective catalysts were selected, and further optimized. To enhance catalyst synthesis and testing, high-throughput experimentation (HTE) and design of experiment (DoE) methodologies were used [27–32].

HTE is based on fast and systematic synthesis and screening of libraries of material samples [32]. The discovery of the first ammonia synthesis at BASF in 1909, followed by a systematic investigation of the periodic table is one of the first striking examples

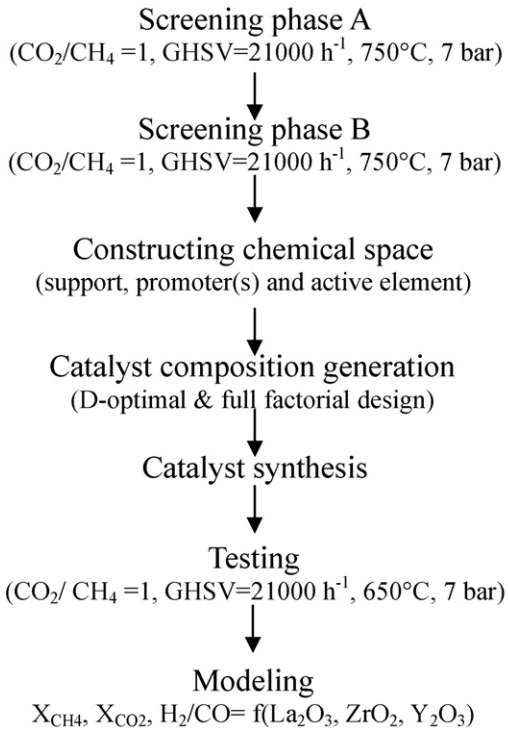

Fig. 1. DoE strategy for the development of dry reforming catalysts at 7 bar.

[33]. DoE intends to maximize the information output with a minimum experimental effort using various strategies. This field of combinatorial chemistry has been successfully applied in material science [27,34–37], heterogeneous [38–40] and homogeneous catalysis [41,42]. Applications to DR are available [43–45].

This contribution evaluates two DoE strategies, *i.e.* full factorial and D-optimal design, for their capability of selecting catalyst compositions, which combine both high activity (on weight basis) and selectivity. Therefore, a chemical space was constructed based on an extensive screening of several active elements, promoters and supports. Next, the two design strategies were used to explore the space and to model the catalytic activity (X_{CH_4}, X_{CO_2}) and selectivity (H_2/CO). With the help of the models the most active and selective catalysts for DR at elevated pressure were identified.

Finally, a critical assessment is given on the choice of the design strategy, *viz.* full factorial *vs.* D-optimal design. The main objective here is the confirmation of the D-optimal principle, *i.e.* maximizing the amount of information from the chemical space through a minimum number of experiments.

2. Experimental

2.1. Design of experiment (DoE)

The DoE strategy for the development of DR catalysts at elevated pressure (7 bar) is summarized in Fig. 1. The first step presents a HT screening carried out in two phases in identical reaction conditions (CO_2/CH_4 = 1, GHSV = 21000 h^{-1}, 750 °C, 7 bar). In phase A, a reference catalyst is designed by selecting a promising active element and support material. Next, different promoters are screened in phase B for their influence on the catalytic performance of the reference catalyst. Three potential promoters were retained for further screening.

A confined chemical space is then constructed with the selected active element, support material and promoters. This space with the selected promoters serving as dimensions is further explored

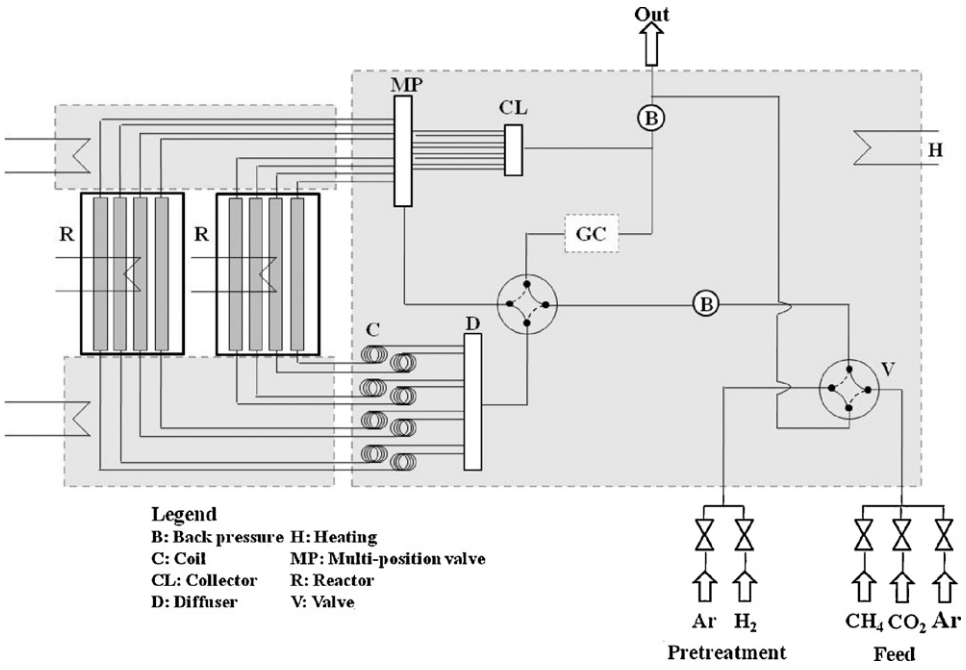

Fig. 2. High pressure reactor set-up. The shaded areas represent heated compartments.

by two different strategies. Both the D-optimal and full factorial design each select a test population out of the candidates within the compositional space. With a full factorial design points at a regular interval in the chemical space are selected, thus corresponding to the intersections of a grid with regular spacing. The D-optimal design uses an algorithm to select a particular test population, which maximizes the amount of information from the chemical space through a minimum number of experiments. This algorithm maximizes the determinant of the information matrix, (X^TX), with X^T being the transposed matrix of X. In the design matrix X each row represents a candidate design point. The D-optimal design and the statistical analysis were carried out with commercially available Design Expert 7 software (Stat-Ease Inc.). After synthesizing and testing the two test populations in the high-pressure reactor unit, catalytic results (X_{CH_4}, X_{CO_2} and H_2/CO) are modeled via ANOVA analyses. Mathematical expressions for each output parameter (X_{CH_4}, X_{CO_2} and H_2/CO) in function of the composition of the catalyst are thus obtained. After model verification, based on a well-chosen objective function, *R*, the most optimal composition can be searched for. Next to the search of the ideal DR catalyst composition, this paper also aims at fair comparison between the two DoE strategies with respect to its reliability and practicability.

2.2. Catalyst preparation

All catalysts were prepared according to reported recipes, except for the calcination process. All catalysts were calcined at 800 °C for 5 h, using a heating rate of 3 °C/min. Catalyst preparation was done using a slurry type impregnation on a HT synthesis platform (see further) [46]. Besides commercially available support materials (TiO_2: Merck; ZrO_2: Chem Lab; γAl_2O_3: Fluka; αAl_2O_3: Alfa Aesar; CaO: Aldrich; $CaCO_3$: Merck; $SrCO_3$: Merck), spinel type XAl_2O_4 (X = Mg, Ca, Sr, Ba) supports were prepared according to an earlier reported recipe [14]. All catalysts are denoted as follows: metal (× wt%) support.

In the D-optimal or full factorial design phase, slurry type impregnation was carried out with a Genesis RSP 100 TECAN liquid handler, available on the HT synthesis platform [46]. Impregnation solutions were prepared by mixing the appropriate volume of stock aqueous solutions of the corresponding metal nitrates (0.2–0.5 M). Distilled water was then added to all vials to obtain an equal impregnation mixture volume of 3 ml. After stirring, 300 mg of the support material was added to the vial containing the impregnation solution. The resulting slurry was then stirred and dried at 70 °C with a H + P Variomag multi-stirring plate. Finally, the obtained powders were calcined at 800 °C for 5 h.

2.3. Catalyst testing and characterization

The catalytic DR reactions are studied at elevated pressure (7 bar) at 750 °C in a continuous downstream flow gas phase reactor, equipped with two parallel fixed bed quadri-reactors placed in two ovens as shown in Fig. 2. Each quadri-reactor contains four parallel alloy 600 fixed bed reactor tubes. Temperatures in both reactor ovens are regulated by a set of thermocouples of type K, placed just above the catalyst bed. The reactor feed, regulated by digital mass flow controllers (Bronkhorst), is equally divided over the eight catalyst beds by a set of coils placed in the valve oven. A multi-position valve selects the reactor tube, from which the products are analyzed using a GC equipped with two 6-way sampling valves. 50 mg of fresh catalyst, pelletized to a 0.125–0.250 mm fraction, is placed on top of a plug of quartz wool.

Reference samples are taken before reaction by passing the reaction feed over each reactor tube at room temperature. These reference samples determine the peak areas of CH_4 and CO_2 in the GC chromatograms at 0% conversion. These values are used to calculate conversion levels at reaction temperature according to $X_{CH_4} = 1 - (\text{area}_{CH_4\ \text{reaction}}/\text{area}_{CH_4\ \text{reference}})$. Blank tests at reaction temperature without catalyst have also been conducted. No significant level of conversion (<1%) was detected during these tests. Next, the catalysts are heated at a heating rate of 5 °C/min till reaction temperature with a non-diluted H_2 stream at rate of 7100 h^{-1} at 7 bar and kept there for 1 h. After pretreatment the reaction is started by passing an equimolar mixture of CH_4 and CO_2 over the catalyst bed at a total pressure of 7 bar. During the screening phase a GHSV of 21000 h^{-1} is used. During the exploration of the constructed chemical space the temperature is set at 650 °C with the GHSV maintained at 21000 h^{-1}. This is done to avoid that the cata-

lysts perform at thermodynamic equilibrium. Feed and products are analyzed with a GC (Trace GC, Interscience), equipped with a back-flush system, and containing two analysis channels. Both channels are equipped with a TCD detector. The first channel is used to analyze CO_2, CH_4 and H_2O via a Porapack column (150 °C) and uses He as reference gas. The second channel with Ar as reference gas uses a Porapack column (65 °C) and a Molsieve 5A (65 °C) column to detect H_2, CO and CH_4. Every 480 s a reactor tube is being analyzed.

To determine the amount of coke deposited during reaction, thermogravimetric analysis (TGA) of spent catalysts is carried out in an oxidative atmosphere ($O_2/N_2 = 9$) with a TGA Q500 of TA instruments equipped with a high-throughput sampling platform designed for 16 samples. The amount of coke is expressed in mol C per mol of methane converted (mol C/mol CH_{4conv}) to allow a fair comparison between the different catalysts. The choice of this unit, and its impact on catalyst design, is explained more in detail elsewhere [47].

3. Results and discussion

3.1. Screening of dry reforming catalysts

As mentioned in Section 1, only a few reports deal with DR at high pressure, most of the catalysts being studied in different reaction conditions. In order to make a fair evaluation, new catalysts were measured in uniform reaction conditions, *viz.* $CO_2/CH_4 = 1$, GHSV = 21000 h^{-1}, 750 °C, 7 bar, using the gas phase HT reactor. As the selected reaction conditions thermodynamically favor coking reactions, differentiation among good and bad catalysts is feasible.

An overview of different active elements, *viz.* Ni, Co and Pt, and support materials, *viz.* TiO_2, ZrO_2, MgO, γAl_2O, CaO, αAl_2O_3, $CaCO_3$, $SrCO_3$, $MgAl_2O_4$, $CaAl_2O_4$, $SrAl_2O_4$ and $BaAl_2O_4$, tested in phase A of the screening is given in Table 1. In Figs. 3 and 4, CO_2 conversion (X_{CO_2}) and syngas molar ratio (H_2/CO) are plotted against CH_4 conversion (X_{CH_4}). Each point corresponds to a single catalyst, numbered according to Table 1. The color code of the individual catalysts denotes the amount of coke (carbon) formed during a reaction time of 2 h. Some catalysts (denoted in black) showed low coking and were overoxidized, as derived from the weight increase during TGA.

Generally, the catalysts cover a broad activity range (Fig. 3). Some catalysts show high activity, reaching the equilibrium conversion in the applied reaction conditions ($X_{CH_4} = 54\%$, $X_{CO_2} = 70\%$), *e.g.* catalysts 20, 21, 24, 28, 31, 32 and 33. A significant number of other catalysts show very low activity, *e.g.* catalysts 3, 9, 11, 12 and 13. All catalysts are located above the diagonal line, representing equal CH_4 and CO_2 conversions, due to the occurrence of the RWGS reaction (3). In addition, the syngas molar product ratio is always below 1, increasing with increasing activity (Fig. 4). This also reflects the occurrence of the RWGS reaction (3). As illustrated by the color legends in both figures, a wide variety of carbon, *viz.* from 0.1 to 50 mmol C per mol CH_4 converted, is deposited on the different catalysts. A clear correlation between the amount of coking (per converted CH_4) and the observed DR activity does not seem to exist.

Whereas $Ni_{0.5}Mg_{0.5}O$ (entry 14) is one of the better performers (high H_2/CO ratio and low coke content) among the reported catalysts (compare with entries 1–4, 9–16 and 18) (Fig. 4), already during the initial screening somewhat better catalyst compositions were noticed. At a first glance, catalysts 20, 21, 24, 28 and 31 seem most promising candidates for coke free DR under high pressure (Table 2). They all approach the thermodynamic conversion in the applied process conditions, while keeping the coke content low (mmol C per mol CH_4 converted <1) (Figs. 3 and 4). With exception of catalyst 28, which contains Co, those catalysts have Ni as the active element. In our hands, the use of a noble metal, *viz.* Pt, was indeed beneficial for DR under high pressure when compared on catalyst weight basis. This catalyst composition is considered to be too expensive to be of relevance for DR (Table 2, compare entry 17 with 25). The metal loading seems to be very crucial for both Ni and Co containing catalysts. When comparing catalysts 24, 28 and 31 with 25, 26, 27, 29 and 30, the composition with higher metal loading, *viz.* 5 wt%, always performs better. On a weight basis, promotion of lower loadings of Ni with CeO_2 seems to activate Ni, especially in combination with γ-alumina as support (compare, *e.g.* entry 25 with entry 20 and 21). A ZrO_2 promoter on Ni/γ-Al_2O_3 favors DR activity (on catalyst weight basis), albeit with more coke formation when compared with a CeO_2 promoter (compare entry 25 and 20 with 22). Finally, based on the initial screening, γ-alumina and spinel structures can be regarded as the support of choice, whereas commercial carbonate supports and other oxides, *viz.* MgO, CaO and ZrO_2, are less suited for developing active and stable DR catalyst (compare entry 25 and 30 with 6, 10, 36, 38 and 39).

Based on these catalytic data, Ni (2.5 wt%) catalyst supported on $MgAl_2O_4$ spinel (entry 30) was selected for the next screening step (phase B) as they combine high DR activity with low coke formation, despite some catalysts in the table performing better either with respect to the DR activity, low coke formation or both, such as entries 24, 28 and 31. As a similar study was recently reported for the same catalyst composition, *viz.* Ni on $MgAl_2O_4$, at atmospheric pressure, we here communicate the promoter effects on the same catalyst at elevated pressure. A comparison between the two studies can be very informative on the influence of promoter effects at different pressures. Besides, as previous research suggests that promoter effects are significant only at high promoter to metal wt% ratios [14,17], the low metal loading, *i.e.* 2.5 wt%, is preferred in order to limit the amount of promoter required on the catalyst. For the lower metal loadings, Ni is the preferred metal (compare entries 26 and 27 with entry 30), while $MgAl_2O_4$ is the preferred support (compare entry 25 with entry 30).

In the phase B, Ni(2.5)$MgAl_2O_4$ catalysts promoted at two levels, *viz.* 2.5 and 5 wt%, were screened. Besides oxides of alkaline (Na, K), alkaline-earth (Mg, Ca, Sr, Ba) and transition metals (Mn, Y, Zr), also lanthanides (La, Ce) were tested as potential modifier for reducing the coke amount. The catalytic results and the corresponding carbon depositions for DR at the elevated pressure are summarized in Table 3.

Addition of alkali oxide promoters (entries 43–46) shows decreased catalyst performance. Addition of Na_2O (entries 43 and 44) has a negative effect on DR activity, as both X_{CH_4} and X_{CO_2} values decrease strongly compared to the unpromoted reference catalyst (entry 30). The Na_2O poisoning effect seems in line with a report by Wang et al. for a γ-Al_2O_3 supported Ni catalyst tested at atmospheric pressure [51]. Promotion with K_2O (entries 45 and 46) in the applied promoter range does not significantly affect the catalyst coke resistance. At atmospheric pressure, promotion with K_2O lowers coking as reported by Luna et al. and Hou et al. [52,53]. Such reported decoking effect of K_2O is not confirmed at the elevated pressure used in this work. In case of alkaline-earth metal oxides, low level (2.5 wt%) promoted catalysts (MgO, CaO, SrO) (entry 47, 49, 51) do not significantly lower catalytic activity, whereas high level promoted catalysts, *viz.* 5 wt% of CaO, SrO and BaO (entries 50, 52 and 54), result in reduced activity. Reduction in activity combined with an increased amount of coking upon promotion with CaO has been reported for a Ni on γ-Al_2O_3 tested at atmospheric pressure [54].

Coking values are substantially reduced in two cases, *i.e.* for Ni(2.5)SrO(2.5)$MgAl_2O_4$ (entry 51) and Ni(2.5)BaO(5)$MgAl_2O_4$ (entry 54). The presence of transition metal oxides, *viz.* MnO, ZrO_2 and Y_2O_3 (entries 55–60), occasionally results in a slight reduction

Table 1
Screening of dry reforming catalysts (CO_2/CH_4 = 1, GHSV = 21000 h^{-1}, 750 °C, 7 bar).

Entry	Catalyst[a]	Ref.[b]	Entry	Catalyst[a]	Ref.[b]
1	$Ni(0.5)TiO_2$	[48]	22	$Ni(2.5)ZrO_2(2.5)\gamma Al_2O_3$	OS
2	$Ni(2.5)TiO_2$	[48]	23	$Ni(2.5)ZrO_2(5)\gamma Al_2O_3$	OS
3	$Co(0.5)TiO_2$	[18,49]	24	$Ni(5)\gamma Al_2O_3$	OS
4	$Co(2.5)TiO_2$	[18,49]	25	$Ni(2.5)\gamma Al_2O_3$	OS
5	$Ni(0.5)ZrO_2$	OS	26	$Co(2)MgAl_2O_4$	OS
6	$Ni(2.5)ZrO_2$	OS	27	$Co(4)MgAl_2O_4$	OS
7	$Co(0.5)ZrO_2$	OS	28	$Co(5)MgAl_2O_4$	OS
8	$Co(2.5)ZrO_2$	OS	29	$Ni(2)MgAl_2O_4$	OS
9	Ni(0.5)MgO	[48]	30	$Ni(2.5)MgAl_2O_4$	OS
10	Ni(2.5)MgO	[48]	31	$Ni(5)MgAl_2O_4$	OS
11	Co(0.5)MgO	[20]	32	$Ni(2.5)CeO_2(2.5)MgAl_2O_4$	OS
12	Co(2.5)MgO	[20]	33	$Ni(2.5)CeO_2(5)MgAl_2O_4$	OS
13	$Ni_{0.15}Mg_{0.85}O$	[48]	34	$Ni(2.5)ZrO_2(2.5)MgAl_2O_4$	OS
14	$Ni_{0.5}Mg_{0.5}O$	[50]	35	$Ni(2.5)ZrO_2(5)MgAl_2O_4$	OS
15	$Co_{0.07}Mg_{0.93}O$	[20]	36	Ni(2.5)CaO	OS
16	$Co_{0.13}Mg_{0.87}O$	[20]	37	$Ni(2.5)\alpha Al_2O_3$	OS
17	$Pt(2.5)\gamma Al_2O_3$	OS	38	$Ni(2.5)CaCO_3$	OS
18	$Pt(2.5)Co(2.5)\gamma Al_2O_3$	[20]	39	$Ni(2.5)SrCO_3$	OS
19	$Co(5)\gamma Al_2O_3$	OS	40	$Ni(2.5)CaAl_2O_4$	OS
20	$Ni(2.5)CeO_2(2.5)\gamma Al_2O_3$	OS	41	$Ni(2.5)SrAl_2O_4$	OS
21	$Ni(2.5)CeO_2(5)\gamma Al_2O_3$	OS	42	$Ni(2.5)BaAl_2O_4$	OS

Subscripts for catalysts 13–16 represent atomic ratios.
[a] Metal (wt%) support.
[b] Reference list; OS: own synthesis procedure.

of catalytic activity. Interestingly, Y_2O_3 (entries 57 and 58), ZrO_2 (entries 59 and 60), and MnO (entry 56) promoters clearly show an increase in coke resistance compared to the unpromoted catalysts. The $Ni(2.5)MnO(2.5)MgAl_2O_4$ catalyst (entry 55) has higher coke amounts in line with $NiMnOAl_2O_3$ catalysts, tested at atmospheric pressure [52]. Y_2O_3 is mainly used in dry reforming research to stabilize a ZrO_2 support, hereby directly influencing the DR activity and selectivity of the metal site via an improvement of the available number of surface oxygen vacancies [55]. The authors have shown reduced coke formation in the presence of Y_2O_3, which is in line with our observation. The beneficial effect of ZrO_2 on the coking resistance of the catalyst is in line with reports at ambient atmosphere [56]. Enhanced CO_2 adsorption at the catalyst surface in the presence of ZrO_2 was given as explanation for the increased catalyst stability.

Finally, two lanthanides, *viz.* La_2O_3 and CeO_2 (entries 61–64) were tested as promoters. While for both lanthanide promoters high catalytic activity is retained, the addition of La_2O_3 shows a substantial increase in coking resistance compared to the reference catalyst, similar to earlier reports at atmospheric pressure [12,51,57]. This increase in coking resistance via La_2O_3 promotion can be explained by the formation of $La_2O_2CO_3$, which is capable of eliminating coke via the reverse Boudouard reaction [57]. In addition, in contrast to dry reforming at atmospheric pressure, at elevated pressure the coke amount is increased upon promotion with CeO_2 [51,58].

Summarizing, a HT screening suggests the use of Ni on $MgAl_2O_4$ as promising catalyst for active and stable DR at elevated pressure. Additional screening of promoted catalysts reveals that effects occurring at atmospheric pressure cannot always be extrapolated

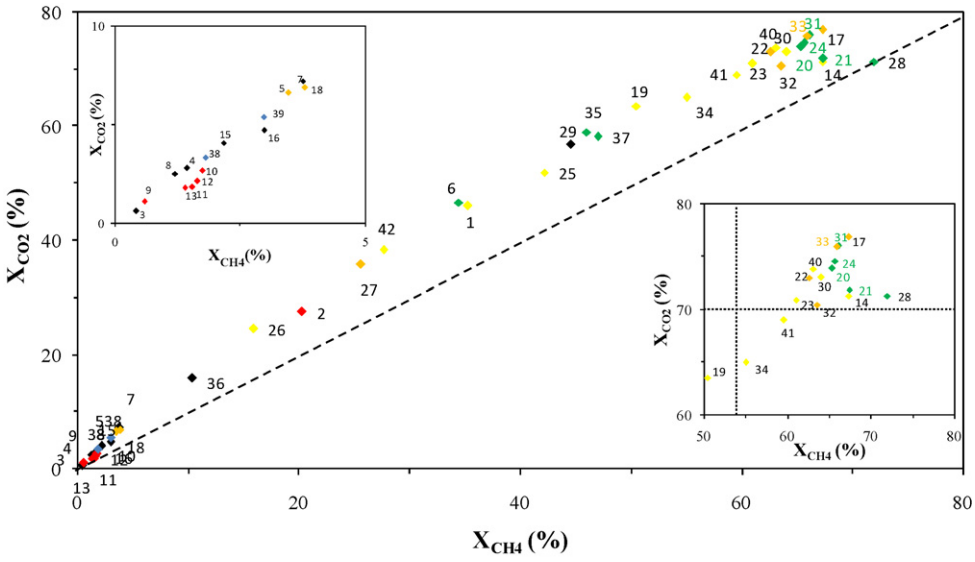

Fig. 3. Carbon dioxide (X_{CO_2}) against methane (X_{CH_4}) conversion and coke of the catalysts from the HT catalyst screening in standard conditions (CO_2/CH_4 = 1, GHSV = 21000 h^{-1}, 750 °C, 7 bar). The amount of carbon, expressed as mmol C per mol converted CH_4 (after 2 h on stream), is denoted by the following color code ♦: no information; ● : <1; ● : 1–4; ● : 4–10; and ● : >10. The dashed line represents equal conversion of both feed gases, while the dotted lines show the feed equilibrium conversions without taking into account carbon deposition. Catalysts are numbered according to Table 1.

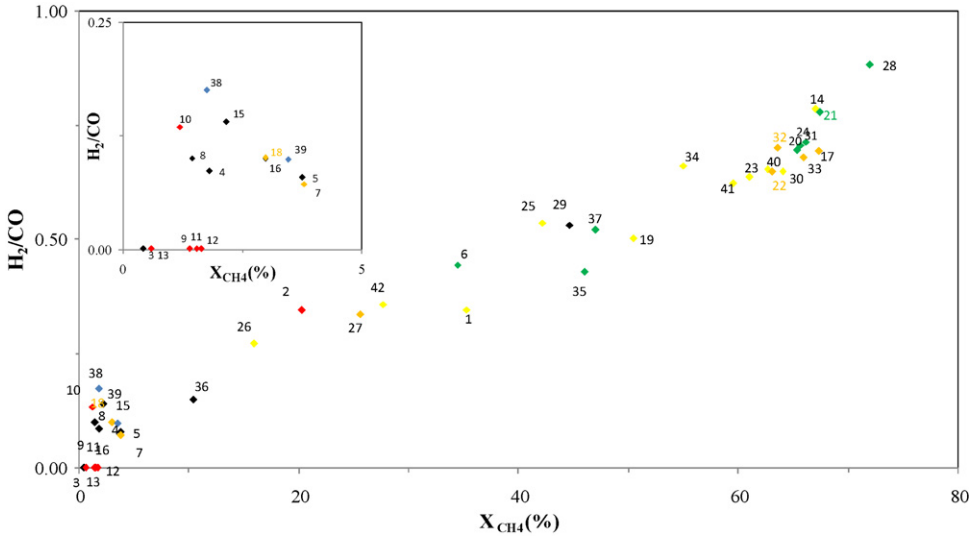

Fig. 4. Syngas product ratio (H_2/CO) against methane conversion (X_{CH_4}), obtained from the HT catalyst screening in standard conditions (CO_2/CH_4 =1, GHSV = 21000 h^{-1}, 750 °C, 7 bar). The amount of carbon, expressed as mmol C per mol converted CH_4 (after 2 h on stream), is denoted by the following color code ♦: no information; ●: <1; ●: 1–4; ●: 4–10; and ●: >10. Catalysts are numbered according to Table 1.

to elevated pressure. BaO, MnO, La_2O_3, ZrO_2 and Y_2O_3 were identified as potential promoters attributing increased coke resistance to the reference catalyst.

3.2. Construction and exploration of the chemical space

In this section two different design strategies, *viz.* D-optimal and full factorial, were compared to achieve new catalyst compositions for DR at elevated pressure. Based on the above information, Ni and $MgAl_2O_4$ were selected as active metal and support, respectively. As mentioned above, the amount of Ni is set at a constant level of 2.5 wt%. Three promoters (La_2O_3, ZrO_2 and Y_2O_3) of the above mentioned list of promising promoters, *viz.* BaO, MnO, La_2O_3, ZrO_2 and Y_2O_3, were arbitrarily selected for the DoE study. The boundaries of the chemical space are set between 0 and 5 wt%, generating a cubic space as depicted in Fig. 5.

To explore this space, both a D-optimal (D) and full factorial (FF) search strategy were applied independently. In case of the D-optimal strategy a cubic model is pre-assumed, since this is the only model which takes into account possible cubic interactions between the three parameters. To maximize the amount of information, catalyst compositions in the whole promoter range were selected out of the candidate list by the D-optimal algorithm as shown in Table 4. Different promoter levels were picked by the algorithm, *viz.* 0, 1.25, 1.67, 2.5, 3.33, 3.75 and 5%, as well as unpromoted, *e.g.* D4, singly, *e.g.* D6 and D9, doubly, *e.g.* D5 and D27, and triply promoted catalysts, *e.g.* D1 and D28. In total, 30 catalyst combinations were tested.

In case of the full factorial strategy, all catalyst combinations compositionally different from each other by 1.66 wt% were selected. This means that all the intersections of a grid with regular spacing of 1.66 wt% in this chemical space were selected (Table 4). Thus, for each promoter four different levels (0, 1.66, 3.33 and 5 wt%), next to all possible combinations of promoters and promoter levels were tested. In total, 64 catalysts were prepared and tested.

Table 2
Conversion of CH_4 (X_{CH_4}) and CO_2 (X_{CO_2}), syngas ratio (H_2/CO) and coke amount (in mmol C per mol CH_4 converted, after 2 h time-on-stream) for a broad selection of catalysts from the first screening (CO_2/CH_4 = 1, GHSV = 21000 h^{-1}, 750 °C, 7 bar).

Entry	Catalyst	X_{CH_4} (%)	X_{CO_2} (%)	H_2/CO	Coke (mmol C/mol CH_{4conv})
6	$Ni(2.5)ZrO_2$	34	47	0.45	0.3
10	$Ni(2.5)MgO$	1	3	0.13	35.2
17	$Pt(2.5)\gamma Al_2O_3$	67	77	0.69	5.5
20	$Ni(2.5)CeO_2(2.5)\gamma Al_2O_3$	65	74	0.70	0.1
21	$Ni(2.5)CeO_2(5)\gamma Al_2O_3$	67	72	0.78	0.1
22	$Ni(2.5)ZrO_2(2.5)\gamma Al_2O_3$	63	73	0.65	7.4
24	$Ni(5)\gamma Al_2O_3$	66	75	0.70	0.1
25	$Ni(2.5)\gamma Al_2O_3$	42	52	0.54	1.1
26	$Co(2)MgAl_2O_4$	16	25	0.27	2.3
27	$Co(4)MgAl_2O_4$	26	36	0.34	5.9
28	$Co(5)MgAl_2O_4$	72	71	0.88	0.2
29	$Ni(2)MgAl_2O_4$	45	57	0.53	n.d.
30	$Ni(2.5)MgAl_2O_4$	64	73	0.65	1.4
31	$Ni(5)MgAl_2O_4$	66	76	0.71	0.3
36	$Ni(2.5)CaO$	10	18	0.15	n.d.
37	$Ni(2.5)\alpha Al_2O_3$	47	58	0.52	0.3
38	$Ni(2.5)CaCO_3$	2	3	0.18	n.d.
39	$Ni(2.5)SrCO_3$	3	5	0.10	n.d.
40	$Ni(2.5)CaAl_2O_4$	63	74	0.65	1.9
41	$Ni(2.5)SrAl_2O_4$	19	24	0.62	2.0
42	$Ni(2.5)BaAl_2O_4$	28	38	0.36	1.4

n.d.: not determined.

Table 3
Conversion of CH_4 (X_{CH_4}) and CO_2 (X_{CO_2}), syngas ratio (H_2/CO) and coke amount of different singly promoted $Ni(2.5)MgAl_2O_4$ catalysts ($CO_2/CH_4 = 1$, GHSV = 21000 h^{-1}, 750 °C, 7 bar).

Entry	Catalyst	X_{CH_4} (%)	X_{CO_2} (%)	H_2/CO	Coke (mmol C/mol CH_{4conv})
30	$Ni(2.5)MgAl_2O_4$[a]	64	73	0.65	1.4
43	$Ni(2.5)Na_2O(2.5)MgAl_2O_4$	4	7	0.10	8.8
44	$Ni(2.5)Na_2O(5)MgAl_2O_4$	2	4	0.07	17.5
45	$Ni(2.5)K_2O(2.5)MgAl_2O_4$	59	70	0.62	2.4
46	$Ni(2.5)K_2O(5)MgAl_2O_4$	66	74	0.70	1.3
47	$Ni(2.5)MgO(2.5)MgAl_2O_4$	59	69	0.61	2.9
48	$Ni(2.5)MgO(5)MgAl_2O_4$	61	71	0.63	6.6
49	$Ni(2.5)CaO(2.5)MgAl_2O_4$	59	69	0.61	2.4
50	$Ni(2.5)CaO(5)MgAl_2O_4$	50	60	0.56	1.7
51	$Ni(2.5)SrO(2.5)MgAl_2O_4$	64	74	0.67	0.8
52	$Ni(2.5)SrO(5)MgAl_2O_4$	56	68	0.60	42.1
53	$Ni(2.5)BaO(2.5)MgAl_2O_4$	49	59	0.55	3.5
54	$Ni(2.5)BaO(5)MgAl_2O_4$	52	63	0.54	0.9
55	$Ni(2.5)MnO(2.5)MgAl_2O_4$	52	64	0.57	4.9
56	$Ni(2.5)MnO(5)MgAl_2O_4$	59	71	0.62	0.5
57	$Ni(2.5)Y_2O_3(2.5)MgAl_2O_4$	62	69	0.70	1.4
58	$Ni(2.5)Y_2O_3(5)MgAl_2O_4$	54	65	0.59	0.5
59	$Ni(2.5)ZrO_2(2.5)MgAl_2O_4$	55	65	0.60	1.1
60	$Ni(2.5)ZrO_2(5)MgAl_2O_4$	46	59	0.54	0.5
61	$Ni(2.5)La_2O_3(2.5)MgAl_2O_4$	65	75	0.66	1.4
62	$Ni(2.5)La_2O_3(5)MgAl_2O_4$	61	68	0.71	0.9
63	$Ni(2.5)CeO_2(2.5)MgAl_2O_4$	62	73	0.65	8.8
64	$Ni(2.5)CeO_2(5)MgAl_2O_4$	66	76	0.68	5.4

[a] Reference catalyst.

The DR activity and selectivity of the catalysts, generated by the two strategies, are evaluated in the high pressure reactor unit at a reactor temperature of 650 °C, a pressure of 7 bar and a GHSV of 21000 h^{-1}. Note that the temperature in the DoE study is deliberately set 100 °C lower than that performed in the initial screening phase, as the unpromoted Ni reference catalyst showed already close to thermodynamic conversion values at 750 °C. In the latter case, a beneficial influence on the DR activity due to catalyst promotion would not be observed. A decrease in feed contact time would be another way to circumvent that the reference catalyst would operate near thermodynamic conversion values at 750 °C. However, this was not an option for our HT reactor set-up since the flow distribution in each of the eight reactors would differ too much. At the lower temperature, the reference catalyst activity is lower than the equilibrium conversions, *viz.* $X_{CH_4} = 31\%$ and $X_{CO_2} = 47\%$, not taking into account carbon deposition.

Table 4
Overview of selected $Ni(2.5)La_2O_3Y_2O_3ZrO_2MgAl_2O_4$ catalysts in case of D-optimal (D) and full factorial (FF) design.

Cat.	La_2O_3[a]	Y_2O_3[a]	ZrO_2[a]	Cat.	La_2O_3[a]	Y_2O_3[a]	ZrO_2[a]	Cat.	La_2O_3[a]	Y_2O_3[a]	ZrO_2[a]
D1	3.75	1.25	3.75	FF1	0.00	0.00	0.00	FF33	3.33	0.00	0.00
D2	1.25	3.75	2.50	FF2	0.00	0.00	1.67	FF34	3.33	0.00	1.67
D3	5.00	2.50	2.50	FF3	0.00	0.00	3.33	FF35	3.33	0.00	3.33
D4	0.00	0.00	0.00	FF4	0.00	0.00	5.00	FF36	3.33	0.00	5.00
D5	0.00	5.00	5.00	FF5	0.00	1.67	0.00	FF37	3.33	1.67	0.00
D6	0.00	2.50	0.00	FF6	0.00	1.67	1.67	FF38	3.33	1.67	1.67
D7	1.67	5.00	0.00	FF7	0.00	1.67	3.33	FF39	3.33	1.67	3.33
D8	0.00	0.00	0.00	FF8	0.00	1.67	5.00	FF40	3.33	1.67	5.00
D9	3.33	0.00	0.00	FF9	0.00	3.33	0.00	FF41	3.33	3.33	0.00
D10	3.75	1.25	1.25	FF10	0.00	3.33	1.67	FF42	3.33	3.33	1.67
D11	5.00	0.00	2.50	FF11	0.00	3.33	3.33	FF43	3.33	3.33	3.33
D12	1.67	5.00	0.00	FF12	0.00	3.33	5.00	FF44	3.33	3.33	5.00
D13	0.00	0.00	3.33	FF13	0.00	5.00	0.00	FF45	3.33	5.00	0.00
D14	0.00	1.67	5.00	FF14	0.00	5.00	1.67	FF46	3.33	5.00	1.67
D15	5.00	0.00	5.00	FF15	0.00	5.00	3.33	FF47	3.33	5.00	3.33
D16	5.00	5.00	0.00	FF16	0.00	5.00	5.00	FF48	3.33	5.00	5.00
D17	3.75	1.25	3.75	FF17	1.67	0.00	0.00	FF49	5.00	0.00	0.00
D18	5.00	1.67	0.00	FF18	1.67	0.00	1.67	FF50	5.00	0.00	1.67
D19	5.00	5.00	0.00	FF19	1.67	0.00	3.33	FF51	5.00	0.00	3.33
D20	2.50	0.00	2.50	FF20	1.67	0.00	5.00	FF52	5.00	0.00	5.00
D21	3.33	5.00	5.00	FF21	1.67	1.67	0.00	FF53	5.00	1.67	0.00
D22	5.00	2.50	5.00	FF22	1.67	1.67	1.67	FF54	5.00	1.67	1.67
D23	0.00	5.00	1.67	FF23	1.67	1.67	3.33	FF55	5.00	1.67	3.33
D24	1.25	1.25	1.25	FF24	1.67	1.67	5.00	FF56	5.00	1.67	5.00
D25	3.75	3.75	1.25	FF25	1.67	3.33	0.00	FF57	5.00	3.33	0.00
D26	1.67	3.33	5.00	FF26	1.67	3.33	1.67	FF58	5.00	3.33	1.67
D27	0.00	5.00	5.00	FF27	1.67	3.33	3.33	FF59	5.00	3.33	3.33
D28	5.00	5.00	3.33	FF28	1.67	3.33	5.00	FF60	5.00	3.33	5.00
D29	2.50	0.00	5.00	FF29	1.67	5.00	0.00	FF61	5.00	5.00	0.00
D30	2.50	2.50	0.00	FF30	1.67	5.00	1.67	FF62	5.00	5.00	1.67
				FF31	1.67	5.00	3.33	FF63	5.00	5.00	3.33
				FF32	1.67	5.00	5.00	FF64	5.00	5.00	5.00

[a] wt%.

Table 5
Conversion of CH_4 (X_{CH_4}) and of CO_2 (X_{CO_2}) and syngas ratio (H_2/CO) for various Ni(2.5)$La_2O_3Y_2O_3ZrO_2MgAl_2O_4$ catalysts selected via D-optimal (D) and full factorial (FF) design (650 °C, 7 bar, CH_4/CO_2 = 1, GHSV = 21000 h^{-1}).

Cat.	X_{CH_4} [a]	X_{CO_2} [a]	H_2/CO	Cat.	X_{CH_4} [a]	X_{CO_2} [a]	H_2/CO	Cat.	X_{CH_4} [a]	X_{CO_2} [a]	H_2/CO
D1	24	33	0.36	FF1	26	33	0.43	FF33	35	44	0.46
D2	22	29	0.37	FF2	6	9	0.15	FF34	32	40	0.49
D3	26	34	0.41	FF3	7	11	0.17	FF35	28	38	0.39
D4	28	37	0.43	FF4	10	15	0.19	FF36	20	28	0.31
D5	7	11	0.15	FF5	7	12	0.15	FF37	30	39	0.41
D6	10	14	0.18	FF6	9	15	0.17	FF38	30	39	0.39
D7	23	31	0.34	FF7	6	11	0.14	FF39	26	34	0.37
D8	26	33	0.43	FF8	11	17	0.21	FF40	27	36	0.37
D9	35	44	0.46	FF9	13	20	0.22	FF41	29	39	0.39
D10	24	32	0.36	FF10	5	9	0.16	FF42	27	36	0.40
D11	27	36	0.39	FF11	6	9	0.20	FF43	21	29	0.36
D12	20	27	0.30	FF12	3	5	0.11	FF44	11	16	0.23
D13	7	11	0.17	FF13	11	16	0.21	FF45	13	19	0.23
D14	11	17	0.21	FF14	15	22	0.13	FF46	11	17	0.22
D15	25	34	0.40	FF15	5	8	0.18	FF47	13	18	0.26
D16	28	53	1.48	FF16	7	11	0.15	FF48	12	19	0.27
D17	10	15	0.29	FF17	22	30	0.36	FF49	28	35	0.42
D18	20	28	0.36	FF18	18	27	0.30	FF50	33	44	0.42
D19	16	23	0.28	FF19	27	33	0.49	FF51	30	40	0.41
D20	21	28	0.34	FF20	29	37	0.43	FF52	25	34	0.40
D21	12	19	0.27	FF21	23	32	0.33	FF53	20	28	0.36
D22	12	18	0.27	FF22	13	20	0.23	FF54	32	42	0.41
D23	15	22	0.13	FF23	16	22	0.29	FF55	34	44	0.44
D24	17	25	0.27	FF24	6	10	0.15	FF56	24	33	0.34
D25	14	21	0.23	FF25	27	35	0.42	FF57	28	37	0.37
D26	11	16	0.23	FF26	14	21	0.27	FF58	28	37	0.37
D27	7	11	0.17	FF27	15	21	0.32	FF59	33	40	0.51
D28	17	23	0.30	FF28	11	16	0.23	FF60	28	37	0.42
D29	11	16	0.21	FF29	20	27	0.30	FF61	28	53	1.48
D30	29	38	0.41	FF30	12	17	0.20	FF62	31	40	0.44
				FF31	6	10	0.16	FF63	17	23	0.30
				FF32	4	7	0.11	FF64	32	41	0.47

[a] %.

The catalytic results in DR at elevated pressure for Ni(2.5)$La_2O_3Y_2O_3ZrO_2MgAl_2O_4$ catalysts selected via a D-optimal and full factorial design are shown in Table 5. The results demonstrate a wide variety in activity, *viz.* X_{CH_4} and X_{CO_2}, and selectivity, *viz.* H_2/CO molar ratio, which makes information extraction easier during ANOVA analyses. From Table 5 it follows already that most catalyst compositions show inferior performance in comparison to the reference catalyst, *viz.* unpromoted Ni (2.5 wt%) on $MgAl_2O_4$, yielding X_{CH_4} of 26%, X_{CO_2} of 33% and H_2/CO of 0.43. General trends typical for DR chemistry can be extracted from the set of catalytic data, thereby validating the reactor set-up and the DoE strategy. First, X_{CO_2} values are higher than X_{CH_4} values for all catalysts, pointing to the occurrence of the RWGS reaction (3). This is also confirmed by the presence of a clear H_2O peak in each chromatogram. Secondly, the data in Table 5 show that the H_2/CO molar ratios increase in parallel with an increase in catalyst activity. Also this observation is in line with the occurrence of the RWGS reaction (3), as CO is produced at the expense of H_2 when the steady-state concentration of CO_2 is high.

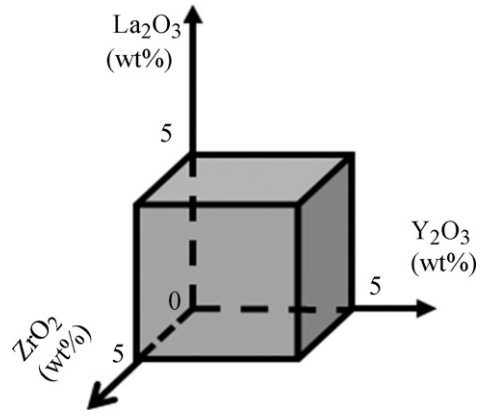

Fig. 5. Chemical space constructed for D-optimal and full factorial exploration.

3.3. Modeling

As shown in Table 6, statistical analyses of the performance (activity and selectivity) of catalysts generated via D-optimal and full factorial design, result in linear equations for the output parameters, *viz.* X_{CH_4}, X_{CO_2} and H_2/CO, as a function of the selected input parameters, *viz.* wt% loading of La_2O_3, Y_2O_3 and ZrO_2. ANOVA analyses showed that the different equations for both designs are statistically significant. More detailed information concerning the modeling and the validity is given in the supplementary information.

These equations, which predict the activity (X_{CH_4}, X_{CO_2}) and selectivity (H_2/CO) for catalysts selected via D-optimal and full factorial design, are visualized in Fig. 6. In these representations all values are expressed relatively compared to the unpromoted Ni(2.5)$MgAl_2O_4$ catalyst, which has a X_{CH_4} value of 26%, a X_{CO_2} value of 33% and a H_2/CO ratio of 0.43.

Table 6
Equations for X_{CH_4}, X_{CO_2}, H_2/CO as a function of La_2O_3, Y_2O_3 and ZrO_2 content of Ni(2.5)$La_2O_3Y_2O_3ZrO_2MgAl_2O_4$ catalysts selected by a D-optimal (D) or full factorial (FF) strategy (650 °C, 7 bar, CH_4/CO_2 = 1, GHSV = 21000 h^{-1}).

D-opt	$X_{CH_4} = 0.88375 + 0.051268La_2O_3 - 0.045449Y_2O_3 - 0.084968ZrO_2$
	$X_{CO_2} = 0.92085 + 0.047189La_2O_3 - 0.044628Y_2O_3 - 0.074943ZrO_2$
	$H_2/CO = 0.80557 + 0.042689La_2O_3 - 0.039035Y_2O_3 - 0.046595ZrO_2$
FF	$X_{CH_4} = 0.64844 + 0.14513La_2O_3 - 0.062361Y_2O_3 - 0.047324ZrO_2$
	$X_{CO_2} = 0.70206 + 0.13971La_2O_3 - 0.059331Y_2O_3 - 0.044714ZrO_2$
	$H_2/CO = 0.63723 + 0.10031La_2O_3 - 0.044815Y_2O_3 - 0.025970ZrO_2$

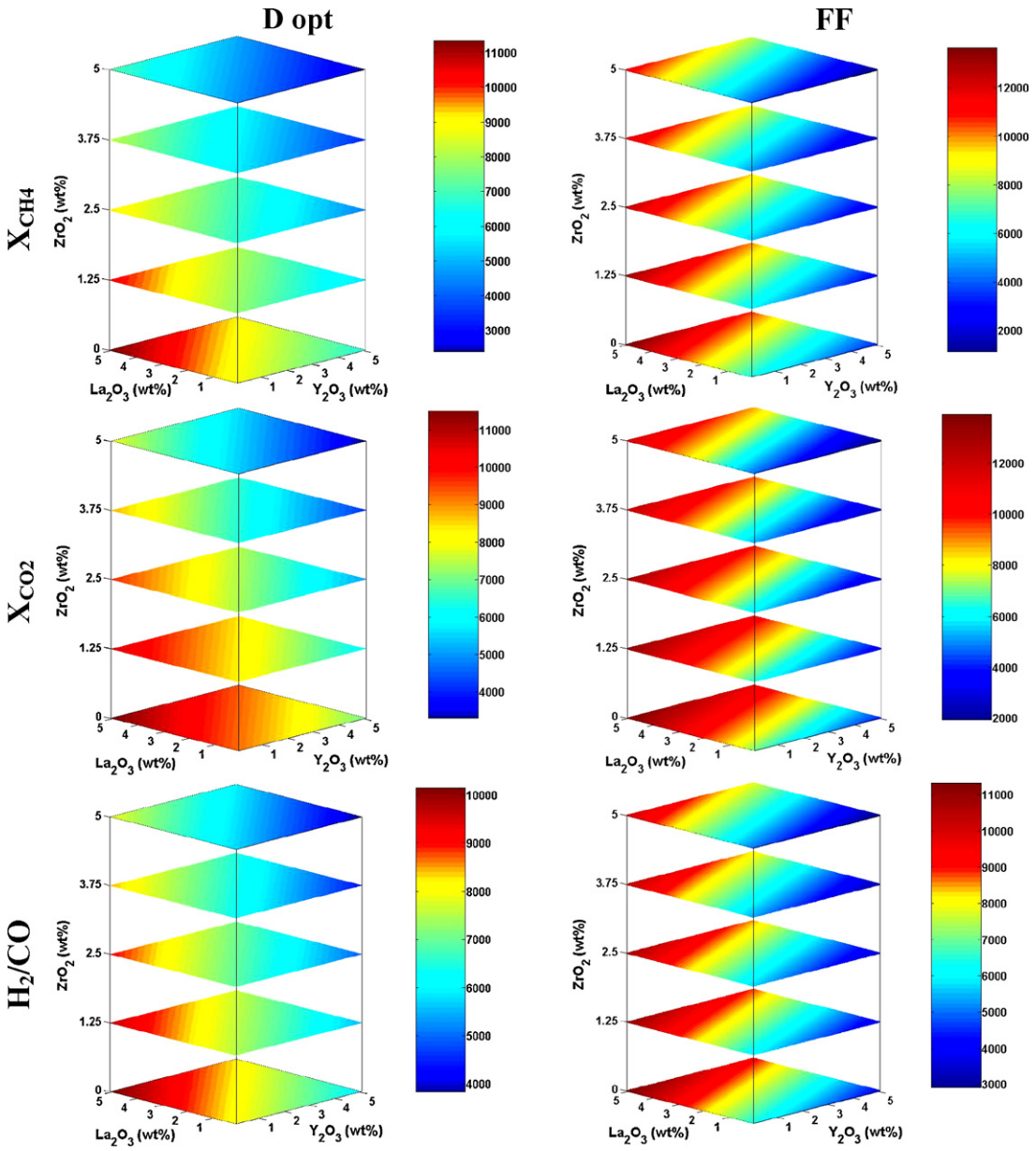

Fig. 6. Visualizations of the equations for X_{CH_4}, X_{CO_2}, H_2/CO of $NiLa_2O_3Y_2O_3ZrO_2MgAl_2O_4$ catalysts obtained via D-optimal and full factorial design (650 °C, 7 bar, $CH_4/CO_2 = 1$, GHSV = 21000 h^{-1}). Values are compared to the reference catalyst $Ni(2.5)MgAl_2O_4$ with $X_{CH_4} = 26\%$, $X_{CO_2} = 33\%$, $H_2/CO = 0.43$. The color codes represent relative values × 10^4.

Generally, it can be seen in these figures that values for X_{CH_4}, X_{CO_2} and H_2/CO are in most cases lower than those of the reference catalyst $Ni(2.5)MgAl_2O_4$. Only when the catalyst contains high loadings of La_2O_3 in the absence of or with only low amounts of the other two additives, significantly higher DR activity is observed. Such conclusion can also be extracted from the data in Table 5. For D-optimal design, in particular catalyst D9 exhibits a DR activity higher than that of the reference, while for full factorial (FF) design FF33, FF34, FF37, FF38, FF49, FF50, FF51, FF54, FF55, FF59, FF62 and FF64 catalysts show higher activities. All catalysts have a high content of La_2O_3 in common.

When the graphs of the two search strategies are compared (Fig. 6), it is clearly seen that the enhanced values for X_{CH_4}, X_{CO_2} and H_2/CO cover a broader compositional range in case of the full factorial design than in case of the D-optimal design. Also the predicted maximum values for the CH_4 and CO_2 conversions and the H_2/CO molar ratio are somewhat higher in case of the full factorial equations.

The effect of each of the promoters can be easily deduced from these visualizations. In case of the D-optimal design, it can be seen that activity (X_{CH_4}, X_{CO_2}) increases when the ZrO_2 content of the catalysts is lowered (appearance of the red color). La_2O_3, as promoter, favorably influences activity (X_{CH_4} and X_{CO_2}) in the whole chemical space considered. As shown in Fig. 6, higher amounts of CO_2 and CH_4 are converted when the La_2O_3 content of the catalyst increases at a fixed level of the two other promoters, Y_2O_3 and ZrO_2. Y_2O_3 has a negative impact on activity since predicted X_{CH_4} and X_{CO_2} values decrease when the Y_2O_3 content increases. The match between the figures of X_{CO_2} and H_2/CO confirms the correlation between high activity and high syngas ratios. As mentioned earlier for catalysts with low activity, syngas ratios are lowered due to the occurrence of the RWGS reaction (3).

In a next step the evaluation of the models is made by comparing P/E values (predicted/experimental) of the 30 catalysts selected via the D-optimal strategy. As shown in Table 7, P/E values for X_{CH_4} all approach a value of 1 except for catalysts D6, D13, D17, D19

Table 7
Overview of P/E ratios for catalysts selected via D-optimal (D) and full factorial (FF) strategies (650 °C, 7 bar, $CH_4/CO_2 = 1$, GHSV = 21000 h^{-1}).

Cat.	X_{CH_4}	X_{CO_2}	H_2/CO	Cat.	X_{CH_4}	X_{CO_2}	H_2/CO	Cat.	X_{CH_4}	X_{CO_2}	H_2/CO
D1	0.8	0.8	0.9	FF1	0.6	0.7	0.6	FF33	0.8	0.9	0.9
D2	0.7	0.7	0.7	FF2	2.7	2.2	1.7	FF34	0.8	0.9	0.8
D3	0.8	0.8	0.8	FF3	1.8	1.6	1.4	FF35	0.9	0.9	1.0
D4	0.8	0.8	0.8	FF4	1.1	1.1	1.2	FF36	1.2	1.1	1.2
D5	0.8	0.9	1.1	FF5	1.9	1.7	1.6	FF37	0.9	0.9	0.9
D6	2.0	1.9	1.7	FF6	1.3	1.2	1.3	FF38	0.8	0.8	0.9
D7	0.8	0.8	0.9	FF7	1.6	1.4	1.4	FF39	0.9	0.9	1.0
D8	0.9	0.9	0.8	FF8	0.7	0.7	0.9	FF40	0.8	0.8	0.9
D9	0.8	0.8	0.9	FF9	0.9	0.8	1.0	FF41	0.8	0.8	0.9
D10	1.0	1.0	1.0	FF10	1.7	1.6	1.2	FF42	0.8	0.8	0.8
D11	0.9	0.9	1.0	FF11	1.3	1.3	0.9	FF43	0.9	0.9	0.9
D12	1.0	0.9	1.0	FF12	1.8	1.9	1.5	FF44	1.7	1.5	1.3
D13	2.2	2.0	1.6	FF13	0.8	0.8	0.8	FF45	1.7	1.5	1.4
D14	0.9	0.9	1.0	FF14	0.4	0.5	1.2	FF46	1.7	1.6	1.4
D15	0.8	0.8	0.8	FF15	0.9	1.1	0.8	FF47	1.4	1.3	1.1
D16	0.9	0.6	0.2	FF16	0.4	0.5	0.8	FF48	1.2	1.1	1.0
D17	1.9	1.7	1.1	FF17	1.0	1.0	1.0	FF49	1.3	1.3	1.2
D18	1.4	1.3	1.1	FF18	1.1	1.1	1.1	FF50	1.0	1.0	1.1
D19	1.5	1.4	1.3	FF19	0.7	0.8	0.6	FF51	1.0	1.0	1.1
D20	1.0	1.0	1.0	FF20	0.6	0.6	0.7	FF52	1.2	1.1	1.1
D21	0.8	0.9	0.8	FF21	0.9	0.9	1.0	FF53	1.6	1.6	1.3
D22	1.3	1.3	1.1	FF22	1.4	1.2	1.3	FF54	1.0	1.0	1.1
D23	0.9	0.9	1.7	FF23	1.0	1.0	0.9	FF55	0.9	0.9	1.0
D24	1.2	1.1	1.2	FF24	2.4	2.0	1.8	FF56	1.1	1.1	1.2
D25	1.5	1.3	1.4	FF25	0.7	0.7	0.7	FF57	1.1	1.1	1.1
D26	1.0	1.0	1.0	FF26	1.1	1.1	1.0	FF58	1.0	1.0	1.1
D27	0.9	1.0	1.0	FF27	0.9	0.9	0.8	FF59	0.8	0.9	0.8
D28	1.0	1.0	0.9	FF28	1.1	1.0	1.0	FF60	0.9	0.9	0.9
D29	1.4	1.4	1.4	FF29	0.8	0.8	0.8	FF61	1.0	0.7	0.3
D30	0.8	0.8	0.9	FF30	1.1	1.1	1.2	FF62	0.8	0.8	0.9
				FF31	1.7	1.6	1.4	FF63	1.4	1.4	1.2
				FF32	2.1	2.0	1.8	FF64	0.7	0.7	0.7

and D25. For these catalysts model predictions exceed experimental observations, demonstrated by high P/E values. For X_{CO_2} and H_2/CO, P/E values deviate from 1 in the case of catalysts D6, D13, D16, D17 and D16, D23. This can be rationalized since D16 has been considered as an outlier during the modeling of X_{CO_2} due to the unrealistic experimental value and is therefore not used for model construction. For the same reason D16 and D23 are not used during modeling of the H_2/CO ratio results. The evaluation using P/E values points out that the proposed mathematical expressions for the majority of the tested catalysts fit the data set generated via the D-optimal strategy.

Similar conclusions can be drawn for the catalysts selected via the full factorial design. La_2O_3 promotion has a positive influence on activity. Like for the D-Optimal design, X_{CH_4} and X_{CO_2} values increase in the whole explored space when the La_2O_3 content is elevated. Maximum activity is reached, just as in case of the D-optimal design, with a $Ni(2.5)La_2O_3(5)MgAl_2O_4$ catalyst. Activity (X_{CH_4}, X_{CO_2}) increases with decreasing ZrO_2 or Y_2O_3 content of the catalysts at constant level of the two other promoters. From Fig. 4 it follows that catalyst activity (X_{CH_4}) and selectivity (H_2/CO) vary in parallel. For the catalysts selected via the full factorial design (Table 7), P/E ratios are seen deviating from 1 for catalysts FF2, FF3, FF5, FF7, FF10, FF11, FF12, FF14, FF16, FF24, FF31, FF32, FF44, FF45, FF46 and FF53 in case of X_{CH_4}, for FF2, FF3, FF5, FF10, FF12, FF24, FF31, FF32, FF45, FF46 and FF53 in case of X_{CO_2} and for FF2, FF5, FF24, FF32 and FF61 in case of H_2/CO. From this list of catalysts only F61 is not used for X_{CO_2} and H_2/CO model construction since it has been defined as an outlier.

The evaluation of the P/E values points out that the equations, shown in Table 6, fit the data for the majority of the catalysts, especially for the equation predicting the H_2/CO ratios. In case of the full factorial analysis, prediction of X_{CH_4} is bad for catalysts with low La_2O_3 content since in the majority of the above-mentioned catalysts (12 out of 16) the La_2O_3 content is below 1.7 wt%. In this area of the chemical space predicted values exceed experimental data.

Differences between the values predicted by the full factorial and the D-optimal strategy are calculated and visualized in Fig. 7. It follows that catalyst composition areas (see yellow, green and light blue areas) exist with high similarity of all output parameters (X_{CH_4}, X_{CO_2}, H_2/CO). The predictive value of the two models for the three output parameters only differs at the border of the chemical parameter space (dark blue and red areas), *i.e.* at low or high La_2O_3 content. However, detailed examination of the 95% confidence intervals (see supplementary information, Tables S2, S3 and S4) points out that these differences are statistically significant only for the output parameters, X_{CH_4} and X_{CO_2}, at high La_2O_3 (>4 wt%) and ZrO_2 (>2.5 wt%) content. Only for this compositional area, the confidence intervals show no overlap.

To further evaluate the two search strategies, the predictive force of the equations from Table 6 is investigated. In Table 8 the predictive force of the D-optimal and full factorial models is demonstrated by calculating P/E values. This calculation is done for catalysts which have not been involved in the construction of the different equations. Fifty-one catalysts selected for full factorial analysis, not used in the D-optimal design, are used to estimate the predictive power of the D-optimal equations. Seventeen catalysts selected for D-optimal strategy, not used for full factorial modeling, are used to investigate the predictive power of the full factorial equations. From the analysis of the P/E ratios (Table 8) similar conclusions can be drawn as formulated for the differences between the values predicted by the two strategies. At low La_2O_3 content (<1.67 wt%, F2–F15 in Table 8) the D-optimal equations predict higher values than the full factorial equations, which in turn are higher than the experimental activity and selectivity values (Table 7). This is easily seen by comparing P/E values in Tables 7 and 8. P/E values for the catalysts, predicted by the D-optimal equations (Table 8), are larger than the predicted values in

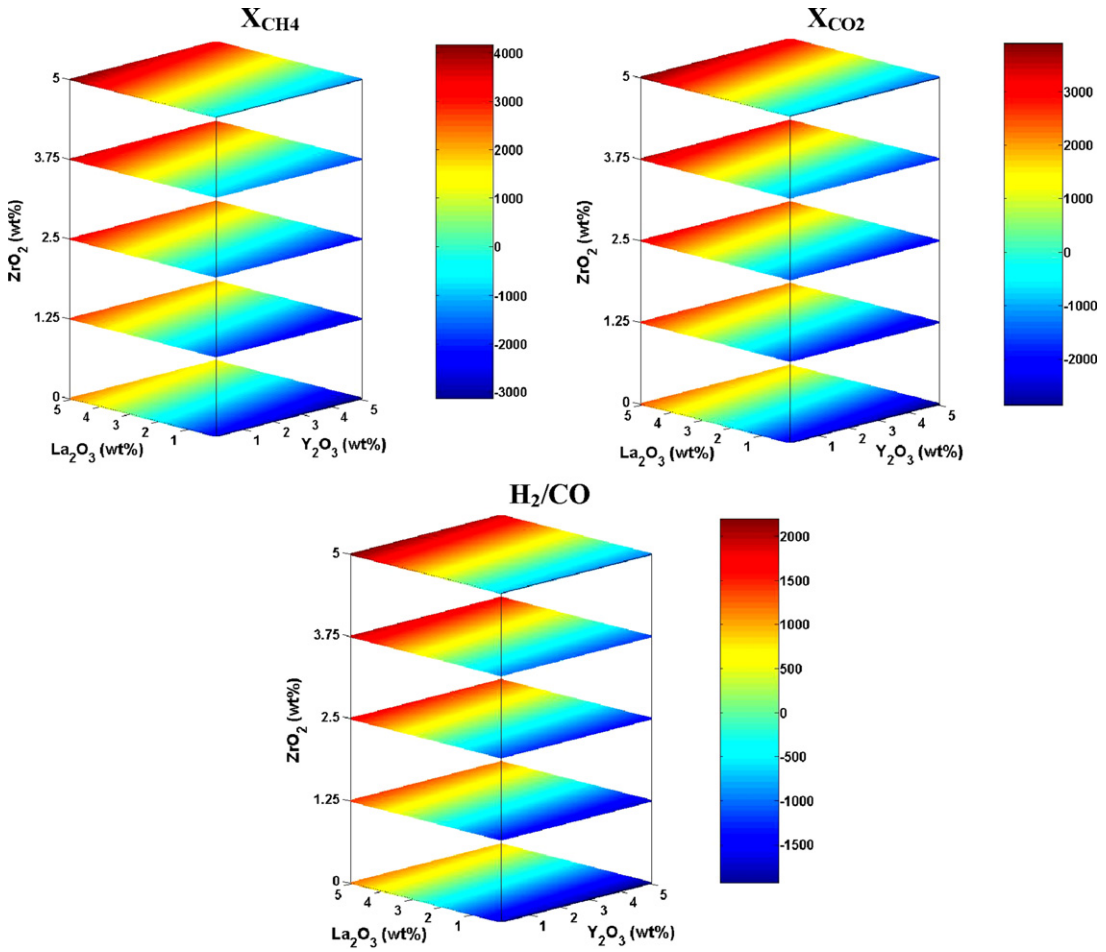

Fig. 7. Calculated differences (FF-D) for X_{CH_4}, X_{CO_2}, H_2/CO values predicted by equations represented in Table 6. Values are compared to the reference catalyst Ni(2.5)$MgAl_2O_4$ with $X_{CH_4} = 26\%$, $X_{CO_2} = 33\%$, $H_2/CO = 0.43$. The color codes represent relative values $\times 10^4$.

Table 7, which are calculated via the full factorial equations. Most P/E values in Table 7 (*e.g.* FF2, FF4, FF5) are higher than 1, indicating that predicted exceed experimental values. It follows that in this region the full factorial strategy delivers superior equations for activity and selectivity prediction. At intermediate La_2O_3 content (1.67–3.33 wt%, FF17–FF48 in Tables 4 and 8), predictions by the equations in both strategies are comparable and fit the experimental results. At high La_2O_3 content (>3.33 wt%, FF48–FF64 in Tables 4 and 8) values predicted by the D-optimal equations are smaller than the experimental ones.

In case of the full factorial equations similar conclusions can be formulated (Table 8). At low La_2O_3 content (D2, D7, D8 and D27) model predictions are usually too low. At high La_2O_3 content (D17, D19, D22 and D25) full factorial equations predict too high the activity and selectivity compared to the obtained experimental values.

In a next step the equations of the two search strategies are compared for a simple case of catalyst composition optimization, aiming at highest activity and selectivity. For this purpose the objective function, R ($R = X_{CH_4} \cdot X_{CO_2} \cdot H_2/CO$), is used. The function R in this case is the product of the values for the conversion of CH_4 (X_{CH_4}) and CO_2 (X_{CO_2}) with the H_2/CO ratio. By maximizing its value, the function R can be used to determine catalyst compositions which combine high activity with high selectivity. Visualization of R values obtained via the two search strategies are given in Fig. 8. It should be noted that the R values span a wide range of values in both strategies, full factorial strategy covering the wider range. However, it is seen in Fig. 8 that for all catalyst composition areas similar trends are present. Low values are predicted in areas which combine presence of ZrO_2 with low La_2O_3 and high Y_2O_3 loading. High values appear in the opposite corner of the space, *i.e.* for ZrO_2 containing catalysts with a low Y_2O_3 and high La_2O_3 content. Optimization based on these models leads towards the same catalyst composition as shown in Fig. 8. In both cases optimization leads to an identical composition, *viz.* Ni(2.5)La_2O_3(5)$MgAl_2O_4$, as most active and selective catalyst.

Conclusively, via ANOVA analyses of the experimental data of catalysts selected via D-optimal and full factorial design, valid mathematical relationships are obtained for the prediction of values for X_{CH_4}, X_{CO_2} and H_2/CO values. In the major part of the confined chemical space comparable values for activity and selectivity are predicted by the equations derived for the two design strategies. Only at the borders of the space differences in predicted values between the two strategies are observed. At low La_2O_3 content, values for the D-optimal design exceed those from the full factorial design, approaching the experimental results better. At high La_2O_3 levels, values from D-optimal design are smaller than experimental values, whereas predicted values for full factorial design approach the experimental values. In both strategies, the impact of the three promoters (La_2O_3, ZrO_2 and Y_2O_3) on activity and selectivity can be predicted easily from the equations. Also compositional optimization yields the same catalyst. Based on these findings, the D-optimal strategy is advantageous compared to the full factorial strategy because in the former case only half the number of experiments is needed. Thus the basic principle of the D-optimal algorithm is confirmed, stating that the D-optimal

Table 8
Overview of P/E ratios predicted by D-optimal and full factorial strategies (650 °C, 7 bar, $CH_4/CO_2 = 1$, GHSV = 21000 h^{-1}).

X_{CH_4}	X_{CO_2}	H_2/CO	Cat.	X_{CH_4}	X_{CO_2}	H_2/CO	Cat.	X_{CH_4}	X_{CO_2}	H_2/CO	X_{CH_4}
FF2	3.7	3.2	2.1	FF35	0.8	0.8	0.9	D1	1.0	1.0	1.0
FF4	1.3	1.4	1.3	FF36	0.9	0.9	1.0	D2	0.6	0.6	0.6
FF5	3.0	2.7	2.2	FF37	0.9	1.0	0.9	D3	1.1	1.1	1.0
FF6	2.1	1.8	1.7	FF38	0.8	0.8	0.9	D6	1.3	1.3	1.3
FF7	2.3	2.0	1.7	FF39	0.8	0.8	0.9	D7	0.7	0.7	0.6
FF9	1.6	1.5	1.3	FF40	0.6	0.6	0.8	D8	0.6	0.7	0.6
FF10	3.0	2.6	1.6	FF41	0.9	0.9	0.9	D10	1.1	1.1	1.1
FF11	2.2	2.1	1.1	FF42	0.8	0.8	0.8	D11	1.2	1.2	1.2
FF12	2.9	3.0	1.8	FF43	0.8	0.9	0.8	D17	2.5	2.2	1.3
FF13	1.6	1.6	1.2	FF44	1.3	1.3	1.1	D19	1.7	1.6	1.4
FF15	2.0	2.1	1.1	FF45	1.8	1.7	1.4	D20	1.1	1.1	1.0
FF17	1.2	1.2	1.1	FF46	1.7	1.6	1.3	D22	2.2	1.9	1.4
FF18	1.3	1.2	1.1	FF47	1.2	1.2	1.0	D24	1.1	1.0	1.1
FF19	0.7	0.8	0.6	FF49	1.2	1.2	1.0	D25	1.7	1.5	1.5
FF20	0.5	0.6	0.6	FF50	0.8	0.9	1.0	D27	0.4	0.6	0.7
FF21	1.1	1.1	1.1	FF51	0.8	0.8	0.9	D29	1.9	1.7	1.5
FF22	1.6	1.5	1.4	FF54	0.8	0.9	0.9	D30	0.8	0.8	0.8
FF23	1.1	1.1	1.0	FF55	0.6	0.7	0.8				
FF24	2.2	2.0	1.7	FF56	0.7	0.8	0.9				
FF25	0.8	0.9	0.8	FF57	1.0	1.0	1.0				
FF26	1.3	1.3	1.1	FF58	0.8	0.9	0.9				
FF27	1.0	1.1	0.8	FF59	0.6	0.7	0.6				
FF30	1.5	1.4	1.3	FF60	0.6	0.6	0.7				
FF31	2.0	1.9	1.5	FF62	0.7	0.7	0.7				
FF32	2.1	2.1	1.8	FF64	0.4	0.5	0.5				
FF34	0.8	0.9	0.8								

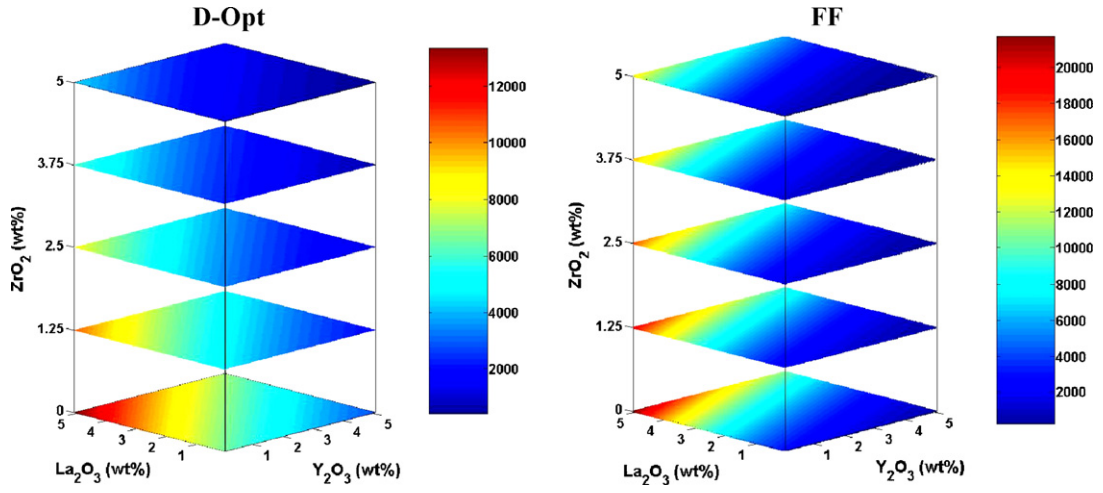

Fig. 8. Visualization of function *R* for catalysts obtained with D-optimal and full factorial design strategy. Values are compared to the reference catalyst $Ni(2.5)MgAl_2O_4$ with $X_{CH_4} = 23\%$, $X_{CO_2} = 33\%$, $H_2/CO = 0.43$. The color codes represent relative values $\times 10^4$.

algorithm maximizes the amount of information with a minimum number of experiments.

4. Conclusions

In this contribution dry reforming catalyst development is explored at elevated pressure. Two search strategies, D-optimal and full factorial, are evaluated for their ability to identify catalysts with high activity and selectivity. For this a DoE has been set up. A high-throughput screening has pointed out that Ni and $MgAl_2O_4$ are the active element and support with high potential for the dry reforming reaction at elevated pressure. A promoter screening of alkaline, alkaline-earth, transition and lanthanide metal oxides shows that promoter effects, reported at atmospheric pressure, not always can be extrapolated to elevated pressure. From a list of promoters, La_2O_3, Y_2O_3, ZrO_2, MnO and BaO were defined as promising elements, while only La_2O_3, Y_2O_3 and ZrO_2 were retained for further use in the DoE.

Next, a cubic space is constructed which is explored using two search strategies. Catalyst compositions are selected via these two strategies and in a next step these catalysts are synthesized and tested. ANOVA analyses of the catalytic activity and selectivity yield equations for X_{CH_4}, X_{CO_2} and H_2/CO for both strategies. After verification, it is shown that, except at the borders of the cubic chemical space, these equations allow prediction of comparable values for X_{CH_4}, X_{CO_2}, H_2/CO in case of the two strategies. Also for both strategies the same effect of the three promoters can be deduced from the equations. La_2O_3 positively influences the activity and selectivity, while the other two promoters, ZrO_2 and Y_2O_3, cause decreased catalyst performance. The search for active and selective catalysts via an objective function, *R*, results in the same catalyst composition for both strategies. These results validate the D-optimal principle and show the advantage of the D-optimal strategy over the full factorial strategy since comparable results are obtained with only half of the number of experiments.

Acknowledgments

S.C. acknowledges a Ph.D. grant from IWT-Vlaanderen. This research is also sponsored by the following research programs: IAP-PAI by BELSPO (Federal Government), GOA, CECAT and long term structural Methusalem funding by the Flemish Regional Government.

Appendix A. Supplementary data

Supplementary data associated with this article can be found, in the online version, at doi:10.1016/j.cattod.2010.06.021.

References

[1] M.C.J. Bradford, M.A. Vannice, Catal. Rev.: Sci. Eng. 41 (1999) 1–42.
[2] J.H. Edwards, A.M. Maitra, Fuel Process. Technol. 42 (2–3) (1995) 269–289.
[3] T. Inui, Appl. Organomet. Chem. 15 (2) (2001) 87–94.
[4] Y.H. Hu, E. Ruckenstein, Catal. Rev.: Sci. Eng. 44 (3) (2002) 423–453.
[5] A.P.E. York, T.-C. Xiao, M.L.H. Green, J.B. Claridge, Catal. Rev.: Sci. Eng 49 (2007) 511–560.
[6] J. Ma, N. Sun, X. Zhang, N. Zhao, F. Xiao, W. Wei, Y. Sun, Catal. Today 148 (2009) 221–231.
[7] T.A. Semelsberger, R.L. Borup, H.L. Greene, J. Power Sources 156 (2) (2006) 497–511.
[8] H.K. Reinius, P. Suomalainen, H. Riihimäki, E. Karvinen, J. Pursiainen, A.O.I. Krause, J. Catal. 199 (2) (2001) 302–308.
[9] A. Haynes, Acetic acid synthesis by catalytic carbonylation of methanol, in: M. Beller (Ed.), Catalytic Carbonylation Reactions, Springer, Berlin, Heidelberg, 2006, pp. 179–205.
[10] N.Q. Minh, Solid State Ionics 174 (1–4) (2004) 271–277.
[11] J.R. Rostrup-Nielsen, Stud. Surf. Sci. Catal. 68 (1991) 85–101.
[12] G.S. Gallego, J.G. Marın, C. Batiot-Dupeyrat, J. Barrault, F. Mondragon, Appl. Catal. A 369 (2009) 97–103.
[13] G. Valderrama, A. Kiennemann, M.R. Goldwasser, Catal. Today 133–135 (2008) 142–148.
[14] S. Corthals, J. Van Nederkassel, J. Geboers, H. De Winne, J. Van Noyen, B. Moens, B.F. Sels, P.A. Jacobs, Catal. Today 138 (2008) 28–32.
[15] A.M. O'Connor, Y. Schuurman, J.R.H. Ross, C. Mirodatos, Catal. Today 115 (1–4) (2006) 191–198.
[16] K. Nagaoka, M. Okamura, K. Aika, Catal. Commun. 2 (2001) 255–260.
[17] K. Nagaoka, K. Seshan, K. Takanabe, K.-I. Aika, Catal. Lett. 99 (2005) 97–100.
[18] K. Nagaoka, K. Takanabe, K.-I. Aika, Appl. Catal. A 268 (1–2) (2004) 151–158.
[19] Y.H. Wang, H. Wang, Y. Li, Q.M. Zhu, B.Q. Xu, in: Symposium on Synthetic Clean Fuels from Natural Gas and Coal-Bed Methane, Sep 07–11, Springer/Plenum Publishers, New York, NY, 2003, pp. 109–116.
[20] K. Omata, N. Nukui, T. Hottai, M. Yamada, Catal. Commun. 5 (12) (2004) 771–775.
[21] S.S Itkulova, K.Z. Zhunusova, G.D. Zakumbaeva, Appl. Organometal. Chem. 14 (12) (2000) 850–852.
[22] J.B. Claridge, A.P.E. York, A.J. Brungs, C. Marquez-Alvarez, J. Sloan, S.C. Tsang, M.L.H. Green, J. Catal. 180 (1) (1998) 85–100.
[23] M.V. Iyer, L.P. Norcio, A. Punnoose, E.L. Kugler, M.S. Seehra, D.B. Dadyburjor, Top. Catal. 29 (3–4) (2004) 197–200.
[24] A.J. Brungs, A.P.E. York, J.B. Claridge, C. Márquez-Alvarez, M.L.H. Green, Catal. Lett. 70 (3) (2000) 117–122.
[25] A. Brungs, A. York, M. Green, Catal. Lett. 57 (1) (1999) 65–69.
[26] D.C. LaMont, A.J. Gilligan, A.R.S. Darujati, A.S. Chellappa, W.J. Thomson, Appl. Catal. A 255 (2) (2003) 239–253.
[27] J.N. Cawse, in: Experimental Design for Combinatorial and High Throughput Materials Development, Wiley, 2003, p. 338.
[28] D. Farrusseng, Surf. Sci. Rep. 63 (2008) 487–513.
[29] L.A. Baumes, P. Collet, Comput. Mater. Sci. 45 (2009) 27–40.
[30] J.M. Serra, A. Corma, S. Valero, E. Argente, V. Botti, QSAR Comb. Sci. 26 (2007) 11–26.
[31] R.J. Hendershot, C.M. Snively, J. Lauterbach, Chem. Eur. J. 11 (2005) 806–814.
[32] Y.L. Dar, Macromol. Rapid Commun. 25 (2004) 34–47.
[33] J.M. Newsam, F. Schuth, Biotechnol. Bioeng. 61 (1999) 203–216.
[34] L. Harmon, J. Mat. Sci. 38 (2003) 4479–4485.
[35] D.C. Webster, Macromol. Chem. Phys. 209 (2008) 237–246.
[36] J.N. Cawse, Acc. Chem. Res. 34 (2001) 213–221.
[37] J.M. Serra, L.A. Baumes, M. Moliner, P. Serna, A. Corma, Comb. Chem. High Throughput Screen. 10 (2007) 13–24.
[38] J.S. Paul, R. Janssens, J.F.M. Denayer, G.V. Baron, P.A. Jacobs, J. Comb. Chem. 7 (2005) 407–413.
[39] J.S. Paul, J. Urschey, P.A. Jacobs, W.F. Maier, F. Verpoort, J. Catal. 220 (2003) 136–145.
[40] W.F. Maier, K. Stöwe, S. Sieg, Angew. Chem. Int. Ed. 46 (2007) 6016–6067.
[41] J.A. Loch, R.H. Crabtee, Pure Appl. Chem. 73 (2001) 119–128.
[42] A. Hagemeyer, B. Jandeleit, Y. Liu, M.P. Damodara, H.W. Turner, A.F. Volpe, W.H. Weinberg, Appl. Catal. A 221 (2001) 23–43.
[43] D.K. Kim, W.F. Maier, J. Catal. 238 (2006) 142–152.
[44] K. Omata, N. Nukui, M. Yamada, Ind. Eng. Chem. Res. 44 (2005) 296–301.
[45] J. Despres, C. Daniel, D. Farrusseng, A.C. van Veen, C. Mirodatos, Stud. Surf. Sci. Catal. 167 (2007) 293–298.
[46] K.P.F. Janssens, J.S. Paul, B.F. Sels, P.A. Jacobs, Appl. Surf. Sci. 254 (2007) 699–703.
[47] S. Corthals, J. Geboers, J. Van Noyen, J. Van Nederkassel, H. De Winne, B. Moens, T. Vosch, X. Ke, H. Poelman, G. Van Tendeloo, J. Hofkens, B.F. Sels, P.A. Jacobs, Design of active and stable $NiCeO_2ZrO_2MgAl_2O_4$ dry reforming catalysts, submitted for publication.
[48] K. Tomishige, Y. Matsuo, Y. Sekine, K. Fujimoto, Catal. Commun. 2 (2001) 11–15.
[49] K. Nagoaka, K. Takanabe, K. Aika, Appl. Catal. A: Gen. 255 (2003) 13–21.
[50] A. Shamsi, Appl. Catal. A: Gen. 277 (2004) 23–30.
[51] S. Wang, G.Q. (Max) Lu, J. Chem. Technol. Biotechnol. 75 (2000) 589–595.
[52] A.E. Castro Luna, M.E. Irearte, Appl. Catal. A 343 (2008) 10–15.
[53] Z. Hou, O. Yokota, T. Tanaka, T. Yashima, Catal. Lett. 87 (2003) 37–41.
[54] Z. Huo, O. Yokota, T. Tanaka, T. Yashima, Appl. Catal. A 253 (2003) 381–387.
[55] J.D.A. Bellido, E.M. Assaf, Appl. Catal. A 352 (2009) 179–187.
[56] Y.-Z. Chen, B.-J. Liaw, W.-H. Lai, Appl. Catal. A 230 (2002) 73–83.
[57] G.S. Gallego, F. Mondragon, J. Barrault, J.-M. Tatibouët, C. Batiot-Dupeyrat, Appl. Catal. A 311 (2006) 164–171.
[58] S. Wang, G.Q. Lu, Appl. Catal. B 19 (1998) 267–277.